Applied Catalysis B: Environmental 202 (2017) 605–610

Contents lists available at ScienceDirect

Applied Catalysis B: Environmental

journal homepage: www.elsevier.com/locate/apcatb

Carbon dioxide Fischer-Tropsch synthesis: A new path to carbon-neutral fuels

Yo Han Choi[a,1], Youn Jeong Jang[b,1], Hunmin Park[b], Won Young Kim[b], Young Hye Lee[b], Sun Hee Choi[c], Jae Sung Lee[d,*]

[a] Division of Advanced Nuclear Engineering, Pohang University of Science and Technology(POSTECH), Pohang 790-784, South Korea
[b] Department of Chemical Engineering, Pohang University of Science and Technology(POSTECH), Pohang 790-784, South Korea
[c] Pohang Accelerator Laboratory, Pohang University of Science and Technology(POSTECH), Pohang 790-784, South Korea
[d] School of Energy and Chemical Engineering, Ulsan National Institute of Science and Technology (UNIST), Ulsan 689-798, South Korea

ARTICLE INFO

Article history:
Received 20 July 2016
Received in revised form
21 September 2016
Accepted 28 September 2016
Available online 29 September 2016

Keywords:
Carbon capture and utilization
Carbon-neutral fuels
Copper-iron catalyst
Liquid hydrocarbons
CO_2 Fischer-Tropsch synthesis

ABSTRACT

Paradigm of climate change mitigation technologies is shifting from carbon capture and storage (CCS) to carbon capture and utilization (CCU). Here we propose a new path to CCU – direct CO_2 conversion to liquid transportation fuels by reacting with renewable hydrogen produced by solar water splitting. The highly promising and CO_2-neutral CCU system is possible by our discovery of a new catalyst that produces liquid hydrocarbon (C_{5+}) selectivity of ~65% and greatly suppressed CH_4 formation to 2–3%, which represents an unprecedented selectivity pattern for direct catalytic CO_2 hydrogenation and is very similar to that of conventional CO-based Fischer-Tropsch (FT) synthesis. The catalyst was prepared by reduction of delafossite-$CuFeO_2$ and *in-situ* carburization to Hägg carbide (χ-Fe_5C_2), the active phase for heavy hydrocarbon formation. The reference catalysts derived from bare Fe_2O_3, CuO-Fe_2O_3 mixture, and spinel $CuFe_2O_4$ are much less active and produce mainly light hydrocarbons, highlighting the critical role of delafossite-$CuFeO_2$ as the catalyst precursor. The new catalyst breaks through the limitation of CO_2-based FT synthesis and will open the avenue for new opportunity for carbon recycling into valuable liquid fuels at the similar conditions to industrially practiced CO-FT synthesis.

© 2016 Elsevier B.V. All rights reserved.

1. Introduction

An unrelenting growth of CO_2 emission into the atmosphere threatens the world's sustainability with the global warming. Carbon capture and storage (CCS) has been considered as the most effective technology of mitigation options. Yet, the past years have observed that storage of CO_2 in a geological reservoir has significant drawbacks of the possible leakage, long-term liability, and availability of enough storage capacity in many regions of the world. Naturally, global interest has been shifting from CCS to carbon capture and utilization (CCU) that converts the captured CO_2 into useful products such as fuels, chemicals, plastics, and alternative building materials [1]. Among proposed options of CCU, conversion of CO_2 into hydrocarbon fuels compatible with our current storage and distribution network is most attractive. It represents a CO_2-neutral path because the fuels turn to CO_2 again upon combustion. Yet, to the extent that the carbon-neutral fuels replace fossil fuels, they result in negative CO_2 emission or net CO_2 removal from the atmosphere. Making hydrocarbons out of CO_2 must overcome two challenges – chemical stability of the CO_2 molecule and a cheap and renewable hydrogen source. Catalytic hydrogenation of CO_2 has been studied intensively, but the products of direct hydrogenation are limited mostly to low molecular weight (C_1-C_4) hydrocarbons or oxygenates (CO, CH_3OH, HCOOH, CH_3OCH_3, *etc.*) instead of heavier liquid hydrocarbons more suitable for transportation fuels [2–10].

Here we propose a new path to CCU – direct CO_2 conversion to liquid fuels with renewable hydrogen produced by solar water splitting as depicted in Scheme 1. Thus, CO_2 emitted from industrial sources like coal power plants, steel mills, or chemical plants is captured and reacts with H_2 generated from solar hydrogen plant to produce liquid fuels in a single step. Our direct CO_2-FT synthesis is different from the CO_2-to-dielsel conversion process recently announced by Audi, which actually involves two steps – reverse water gas shift (RWGS) reaction to CO followed by CO Fisher-Tropsch (FT) synthesis [11]. The solar water splitting to produce hydrogen is developing rapidly lately and highly efficient

* Corresponding author.
E-mail address: jlee1234@unist.ac.kr (J.S. Lee).
[1] These authors contributed equally to this work.

http://dx.doi.org/10.1016/j.apcatb.2016.09.072
0926-3373/© 2016 Elsevier B.V. All rights reserved.

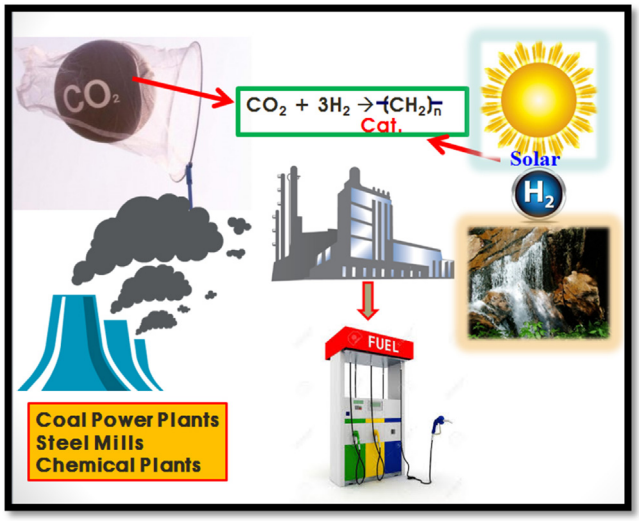

Scheme 1. Proposed carbon capture and utilization (CCU) system based on catalytic CO_2 conversion to liquid hydrocarbon fuels with hydrogen supplied from solar water splitting.

PV-electrolysis [12] or photoelectrochemical systems [13,14] have been developed. Hence, this report focusses on the catalytic CO_2-to-liquid fuel conversion (CO_2 FT synthesis) with renewable H_2.

Hydrogenation of CO_2 to hydrocarbons consists of two reactions in series – RWGS reaction (Eq. (1)) and FT synthesis (Eq. (2)) [15].

$$CO_2 + H_2 \leftrightarrow CO + H_2O \Delta H_{298} = +41\ kJ/mol \quad (1)$$

$$CO + 2H_2 \rightarrow (-CH_2-)_n + H_2O \Delta H_{298} = -152\ kJ/mol \quad (2)$$

Compared to conventional CO-FT reaction with synthesis gas (a mixture of CO and H_2), CO_2 hydrogenation involves three moles of hydrogen per mole of CO_2 and produces plenty of byproduct water, which is a deactivation agent for iron-based FT catalysts. Hence, CO_2 hydrogenation is much slower than CO-FT reaction under the same conditions [15]. The hydrocarbon products include light hydrocarbons (C_1-C_4 paraffins and olefins), and heavier hydrocarbons (C_5^+), and oxygenates [16]. Because CO is the chain growing agent in FT reaction, CO_2 hydrogenation produces mainly low molecular weight hydrocarbons instead of C_5^+ products that are more valuable as liquid transportation fuels.

The CO_2 hydrogenation to hydrocarbons has been studied mainly on traditional catalysts for CO-FT synthesis and Fe-based catalysts are favored over Co, Ni and Ru because of their RWGS activity and relatively higher selectivity for C_2^+ hydrocarbons. The selectivity of Fe catalysts for C_5^+ products could be further improved by employing proper promoters. Widely studied promoters to tailor the product distribution of Fe catalysts include second metals (Mn, Cu, La, Zr, Cr, Mo, or Ta), alkaline metals (Na, K, or Rb), and metal oxides (α-Al_2O_3 and TiO_2) [7,17–23]. In spite of improvement by these promoters, the selectivity for C_5^+ hydrocarbons is much lower than that obtained from CO-FT synthesis over similar catalysts.

Our novel Cu—Fe catalyst derived from delafossite-$CuFeO_2$ produces heavy hydrocarbons from CO_2 hydrogenation in the same manner as from conventional CO-FT synthesis. Thus, reduction and *in-situ* carburization $CuFeO_2$ formed effectively the Hägg iron carbide (χ-Fe_5C_2), the known active catalytic phase for the formation of heavier hydrocarbons in FT synthesis. The unique role of delafossite-$CuFeO_2$ as the catalyst precursor is evident because Cu—Fe reference catalysts derived from Cu_2O-Fe_2O_3 mixture and spinel $CuFe_2O_4$ were much less active and produced mainly light hydrocarbons highlighting the critical role of delafossite-$CuFeO_2$ as the catalyst precursor.

2. Experimental

2.1. Catalyst preparation

Delafossite-$CuFeO_2$ was prepared by a simple hydrothermal method according to a reported procedure [24–26]. Thus, 2.02 g of $Fe(NO_3)_3 \cdot 9H_2O$ and 1.2 g of $Cu(NO_3)_2 \cdot 3H_2O$ were dissolved in 40 ml of distilled water and then 0.1 mol NaOH was added into the solution to maintain the basic condition. After stirring for 30 min, 0.5 ml of propionaldehyde was added as reduction agent for copper (II) to copper (I). The mixture was transferred to 100 ml Teflon-lined stainless steel autoclave and hydrothermal reaction took place at 180 °C for 6–24 h. The synthesized products are designated as $CuFeO_2$-6, $CuFeO_2$-12, and $CuFeO_2$-24 depending on the synthesis time of 6, 12 and 24 h, respectively. Spinel $CuFe_2O_4$ nanopowders (<100 nm) was purchased from Sigma-Aldrich and bare Fe_2O_3 from Kanto, and used as received. All the prepared catalysts are denoted by their precursors, *i.e.* ex-$CuFeO_2$, ex-$CuFe_2O_4$, and ex-Fe_2O_3

2.2. Catalytic CO_2 hydrogenation

The catalytic CO_2 hydrogenation was carried out in a fixed bed, stainless steel reactor with a CO_2/H_2 ratio of 1:3. The pre-reduction was performed under 100 sccm of pure H_2 at 400 °C for 2 h. For catalytic reaction, CO_2 and H_2 were supplied into reactor with N_2 as an internal standard gas to calculate CO_2 conversion. The reaction conditions were 300 °C, 10 bar and a gas hourly space velocity (GHSV) of 1800 ml g^{-1} h^{-1}. Concentrations of the CO_2, CO products and N_2 were measured by an on-lined Agilent 7890A gas chromatograph with a thermal conductivity detector and a Carboxen 1000 packed column. Hydrocarbons of C_1-C_6 were analyzed with the same GC with a flame ionization detector and an Alumina Sulfate PLOT Capillary column. The heavier hydrocarbon products were collected in cold trap. The composition of the heavy hydrocarbons was calculated on weight percent of carbon number by using simulated distillation (SIMDIS) analysis.

2.3. Characterization and product analysis

High-resolution transmission electron microscopy (HR-TEM) and scanning electron microscopy (SEM) were carried out on JEOL JEM-2200FS and Philips Electron Optics B. V. XL30S FEG, operated at 10 k eV. Powder X-ray diffraction (XRD) patterns were collected from PANalytical x'pert using Cu Kα radiation. Temperature-programmed reduction (H_2-TPR) was performed on an AutoChem II apparatus of Micromeritics. Pore size distribution and BET surface area were analyzed by N_2 sorption isotherms measured at 77 K on Mirae SI, Nanoporosity-XQ apparatus. X-ray photoelectron spectroscopy (XPS) was carried out on ESCALAB 250×i using Al Kα radiation.

X-ray asborption fine structure (XAFS) experiments were carried out on 7D beamline of Pohang Accelerator Laboratory (PLS-II, 3.0 GeV, 400 mA). The synchrotron radiation was monochromatized using a Si(111) double crystal monochromators. At room temperature, spectra for the Fe K-edge (E_0 = 7112 eV) and the Cu K-edge (E_0 = 8979 eV) were taken in a transmission mode. The incident beam was detuned by 30% for the Fe K-edge and by 20% for the Cu K-edge in order to minimize contamination of higher harmonics and its intensity was monitored using He-filled and N_2-filled IC SPEC ionization chambers for Fe and Cu K-edges, respectively. For each sample, a reference spectrum of Fe foil or Cu foil was recorded simultaneously so that the energy in the spectrum of sample could be calibrated with respect to the K-edge energy of Fe metal or Cu metal. The AHENA in the IFEFFIT suite of programs was used to ana-

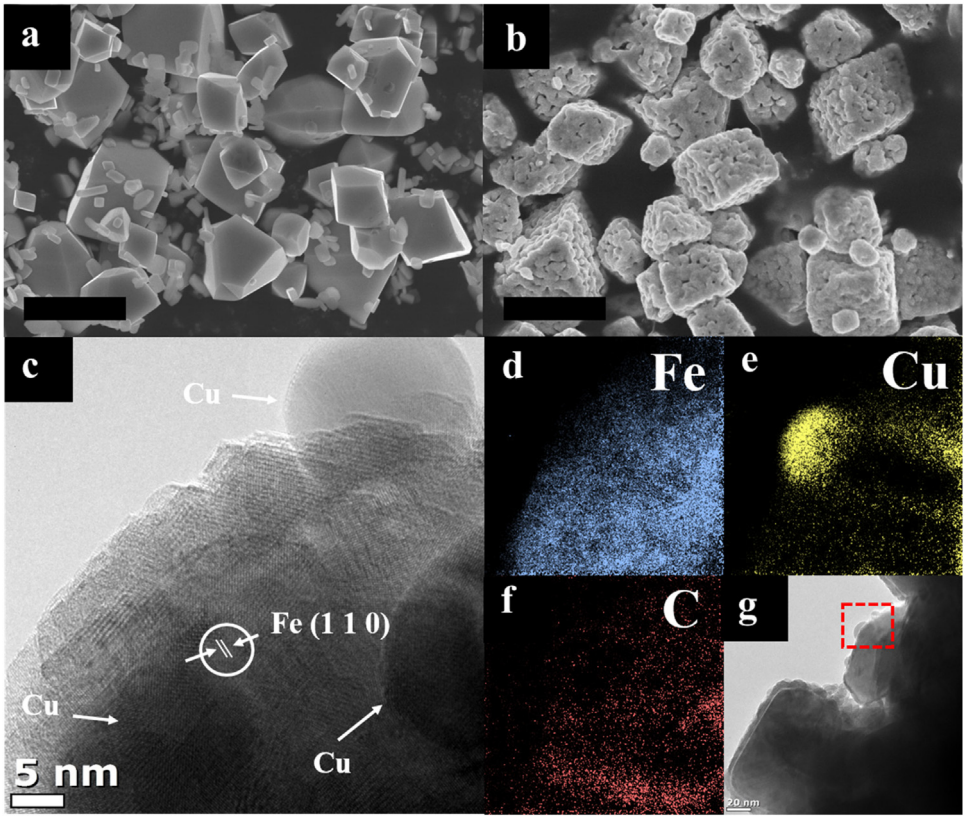

Fig. 1. SEM images of rhomboheral $CuFeO_2$ crystals synthesized by hydrothermal reaction for 12 h (a) and $CuFeO_2$-12 reduced by H_2 (b) (scale bar, 2.5 μm). HR-TEM images of reduced $CuFeO_2$-12 (c), and EELS mapping images of Fe (d), Cu (e) and C (f) for indicated area in the image in (g) of the used $CuFeO_2$-12.

lyze the obatined data to determine the local structures of Fe and Cu in $CuFeO_2$, $CuFe_2O_4$ and Fe_2O_3 catalysts.

3. Results

3.1. Physicochemical properties of the catalysts

As described in Experimental, delafossite-$CuFeO_2$ was synthesized by a hydrothermal method according to a reported procedure [24–26]. The catalyst precursor has delafossite $CuFeO_2$ structure as shown by the XRD pattern (JCPDS card 01-075-2146) in Fig. S1 of Supporting information (SI). The impurity phases of Fe_2O_3 and Cu_2O are also observed with main diffraction peaks at $2\theta = 33$ and 38.9°, respectively, but their intensity gets diminished as the hydrothermal time increases from 6 to 24 h. All the $CuFeO_2$ samples reduced at 400 °C for 2 h exhibit two intense diffraction peaks at 43.3 and 44.7° identified as Cu and Fe metals, respectively (Fig. S1b). The same metallic phases are also observed for reduced $CuFe_2O_4$ of the original inverse spinel structure, but Fe in this reference catalyst has a higher intensity. Thus both $CuFeO_2$ and $CuFe_2O_4$ form separate phases of metallic Cu and Fe upon reduction.

Morphological details of synthesized catalysts were analyzed by scanning and transmission electron microscopy (SEM, TEM). As shown in Figs. 1 and S2, $CuFeO_2$ forms rhombohedral crystals of ~1.0 μm together with many smaller particles of Cu_2O and Fe_2O_3 impurities that join into $CuFeO_2$ crystals with extended hydrothermal reaction following an Ostwald ripening process. This hydrothermal method allows easy synthesis of crystalline $CuFeO_2$ at a low temperature compared to other synthesis methods [27,28]. Upon reduction, many macropores are developed in $CuFeO_2$ particles with the original rhombohedral morphology and size preserved (Fig. 1b). The evolution of textural properties extracted from N_2 adsorption-desorption isotherms is presented in Figs. S3–S4 and Table S1 of SI. The reference spinel $CuFe_2O_4$ (Sigma-Aldrich) is made of small nanoparticles of 30–50 nm (Fig. S5). Fig. 1c exhibits HR-TEM images of reduced $CuFeO_2$ with H_2, where spherical copper particles of ~20 nm in diameter are formed in contact with iron particles of irregular shape. Electron energy loss spectroscopy (EELS) mapping of $CuFeO_2$–derived catalyst after the CO_2 hydrogenation at 300 °C for 16 h in Fig. 1d–f indicates that carbon is well dispersed overlapping with the distribution of Fe, but no correspondence with Cu distribution. This could be taken as an initial sign of the iron carbide formation in $CuFeO_2$–derived catalyst as discussed below.

3.2. Catalytic $CO_2 + H_2$ reactions

The prepared catalysts were investigated for $CO_2 + H_2$ reactions in a fixed bed, stainless steel reactor at 300 °C, 10 bar with $H_2/CO_2 = 3$ and a gas hourly space velocity (GHSV) of 1800 ml g^{-1} h^{-1}. Three reference catalysts were tested derived from spinel-$CuFe_2O_4$, Fe_2O_3, and 1:1 physical mixture of Cu_2O-Fe_2O_3. The time curves and product distributions are summarized in Fig. 2 and Table 1. The reaction rates are expressed in Fe time yield (FTY = mol of CO_2 converted per g of Fe in the catalyst per second). The FTY remains stable after an early induction period of *ca.* 2 h. The FTY values are lower than typical values of CO hydrogenation on Fe-based catalysts by a factor of ~10 [29]. Their performance is compared with reported values for CO_2 hydrogenation over iron-based catalysts in Table S2 of SI. FTY of ex-$CuFeO_2$ is at least 2 times higher than other unsupported reference catalysts studied here. All catalysts have similar CO selectivity around 30% by the RWGS reaction. It indicates that Fe metal has a similar RWGS activity with or without copper. The most remarkable observation in Table 1 is

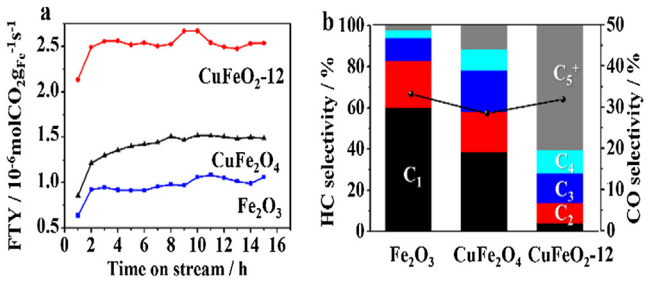

Fig. 2. (a) Fe time yield (FTY) against time on stream for catalysts derived from Fe_2O_3, $CuFe_2O_4$, and $CuFeO_2$-12 precursors. (Reaction conditions: 300 °C, 10 bar, 1800 ml g^{-1} h^{-1}, $H_2/CO_2 = 3$). (b) Product selectivity on CO-free basis.

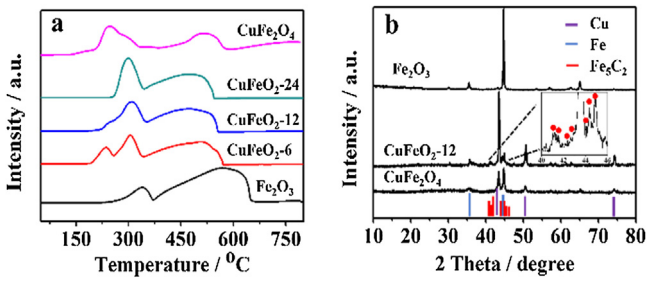

Fig. 3. (a) Temperature-programmed reduction (TPR) profile of various catalyst precursors. (b) XRD patterns after CO_2 hydrogenation at 300 °C for 16 h. The bottom panel indicates expected peak positions for Cu, Fe, and Fe_5C_2. Inset shows expanded pattern of ex-$CuFeO_2$-12 with χ-Fe_5C_2 peaks highlighted.

that ex-$CuFeO_2$ catalyst exhibits extraordinary selectivity toward heavier hydrocarbons (C_5^+) and olefins. The C_5^+ selectivity higher than 65% is typically observed for CO-FT synthesis over iron-based catalysts, yet has never been reported so far in CO_2 hydrogenation as shown in Table S2. Equally impressive is the very low (2–3%) methane selectivity, which is also unusual in CO_2 hydrogenation. The ex-$CuFeO_2$ catalyst also shows a very high olefin-to-paraffin (O/P) ratio of 7.3 for C_2-C_4 hydrocarbons. Fig. S6 of SI represents the carbon number analysis using a simulated distillation method for liquid products collected from CO_2 hydrogenation over ex-$CuFeO_2$. The main products cover the gasoline (C_5-C_{11}) and diesel (C_{12}-C_{21}) ranges, while waxy hydrocarbons (C_{25}^+) are ~15 wt%. The product distribution is very similar to the one typically observed in CO-FT synthesis over iron catalysts [30].

The unique selectivity of ex-$CuFeO_2$ is evident in comparison with reference catalysts under the same conditions. First, the catalyst derived from Cu_2O (Alfa) did not show any CO_2 conversion at all indicating no activity for RWGS. Next, a physical mixture of Cu_2O-Fe_2O_3 (weight ratio = 1:1) manifests much lower CO_2 conversion, very little C_5^+ selectivity and small O/P ratio compared to ex-$CuFeO_2$. The product distribution is very similar to ex-Fe_2O_3 with no obvious beneficial effects of copper. Finally, the catalyst from spinel-$CuFe_2O_4$ with copper in the structure shows improved C_5^+ selectivity and O/P ratio, but only marginally. Alkali metals such as K and Na are usually introduced to iron catalysts in order to promote olefin selectivity in CO_2 hydrogenation. Our catalyst is unique in producing the high O/P ratio with no added alkali metal. The ICP analysis showed that ex-$CuFeO_2$ contained only 0.03% of Na residue from the preparation step, which is much lower than typical alkali-promoted iron catalysts. Thus there must be unique roles of delafossite $CuFeO_2$ as the catalyst precursor, not simply as a source of copper.

Additional kinetic studies were carried out for the ex-$CuFeO_2$ catalyst to find the effect of GHSV (Table S3) and CO/CO_2-cofeeding (Table S4). Pure CO hydrogenation shows a high CO conversion of 80.9% with increased FTY by a factor of 4.2. But the unique selectivity pattern (high C_5^+ selectivity, high O/P ration, and low methane selectivity) remain similar. The results confirm that our ex-$CuFeO_2$ catalyst shows very similar product distribution in the hydrogenation of both CO_2 and CO. Hence, our catalyst could be used as an efficient CO-FT synthesis catalyst as well. A longer term stability test in Fig. S7 indicates that the CO_2 conversion and C_5^+ selectivity remains invariant for 100 h on stream.

3.3. Unique role of delafossite-$CuFeO_2$ as the catalyst precursor

In this work, a novel Cu—Fe catalyst derived from delafossite-$CuFeO_2$ produces heavy liquid hydrocarbons and olefins selectively from CO_2 hydrogenation just like CO-FT synthesis. This represents the first demonstration that liquid fuels and olefins of high value and large market could be obtained directly from CO_2, the most troublesome greenhouse gas. In addition to the practical significance, it is fundamentally interesting that Cu—Fe catalysts derived from Cu_2O-Fe_2O_3 mixture and spinel $CuFe_2O_4$ are much less active and produce mainly light paraffins, in spite of the similar Cu—Fe—O compositions in the form of a physical mixture as well as the crystal structure. Thus the unique product distributions could be obtained only when delafossite-$CuFeO_2$ is used as the catalyst precursor. A small amount of copper metal (typical molar ratio of Cu/Fe = 0.03-0.07) has long been used as a promoter for iron catalysts in CO-FT synthesis, where it serves as a reduction promoter facilitating the reduction of Fe^{3+} as well as carburization of Fe by CO/H_2 during the pretreatment or catalytic reaction. It is also reported that copper affects the performance of iron-based catalyst during the FT reaction as a separate metallic phase [31] or Cu^+ phase [32]. But any of the previous works cannot explain the dramatic precursor effect observed in this work.

In order to clarify the role of copper, the reducibility of the precursors was studied with temperature-programmed reduction (H_2-TPR) analysis in Fig. 3a. The TPR pattern of bare Fe_2O_3 catalyst shows the peaks at 340 and 560 °C, similar to the reported results [33]. All $CuFeO_2$ catalysts have distinctly lower reduction temperatures, indicating that copper promotes the reduction of

Table 1
CO_2 conversion and selectivity for catalysts derived from various precursors[a].

Catalyst	CO_2 Conv.[%]	CO sel.[%]	CO-free HC sel.[%]					O/P[c]
			C_1	C_2	C_3	C_4	C_{5+}	
Fe_2O_3	14.3	33.2	60.2	22.5	11.3	3.7	2.3	0.03
$CuFeO_2$-6	17.3	31.7	2.7	8.3	12.6	10.1	66.3	7.3
$CuFeO_2$-12	18.1	31.9	3.9	10	14.5	11.3	60.3	7.0
$CuFeO_2$-24	16.7	31.4	2.4	8.7	13.3	10.7	64.9	7.7
$CuFe_2O_4$	13.3	28.4	38.3	19.7	20.1	10.5	11.4	0.02
Cu_2O-Fe_2O_3[b]	15.7	28.9	57.6	22.8	12.6	4.4	2.6	0.03

[a] Selectivity was calculated on CO-free basis.
[b] Physically mixed Cu_2O and Fe_2O_3 (weight ratio = 1:1).
[c] Olefins/parafins ratio of C_2-C_4 products.

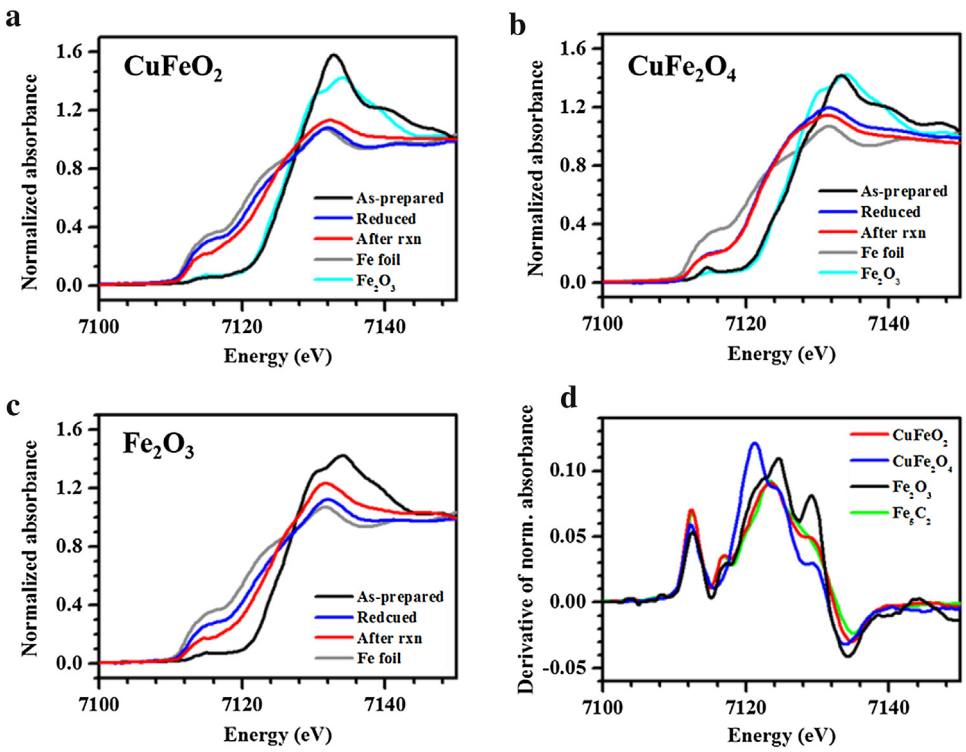

Fig. 4. Fe K-edge XANES spectra (a-c) and derivative spectra of normalized absorption (d) of iron-based catalysts: (a) $CuFeO_2$, (b) $CuFe_2O_4$, (c) Fe_2O_3, (d) after reaction for 16 h.

iron as reported. The shoulder peak at 240 °C for $CuFeO_2$-6 represents the reduction of impurity Cu_2O phase to Cu^0. The peak intensity decreases with increasing synthesis time from 6 to 24 h. Spinel $CuFe_2O_4$ starts its first reduction of Cu in a lower temperature <250 °C. Reduction of iron in $CuFe_2O_4$ begins between 400 and 450 °C, which is consistent with the reported reduction temperature of Fe^{3+} to Fe^{2+} [34], and complete reduction to metallic Fe is observed ~650 °C. The final reduction temperature is significantly higher than that of $CuFeO_2$ (~550 °C) though both catalysts contain reduction promoter Cu. Hence, the reducibility to metallic state is higher for $CuFeO_2$ than $CuFe_2O_4$.

Another proposed role of copper is to facilitate the *in-situ* carburization iron to the active carbide phase during the CO_2 hydrogenation. The XRD analysis in Fig. 3b after CO_2 hydrogenation at 300 °C for 16 h indicates that ex-$CuFeO_2$ catalyst has the doublet peaks at the similar positions of reduced catalysts, but the intensity of Fe peak is greatly reduced and many small new peaks appear, which are identified as diffraction peaks of Hägg iron carbide (χ-Fe_5C_2) as highlighted in the inset. In ex-$CuFe_2O_4$ catalyst, the intensity of Fe metal peak is reduced, but the formation of the carbide could not be identified. No particular change is observed for the used ex-Fe_2O_3 catalyst after the reaction. Post-reaction XPS analysis in Fig. S8 reveals that both of Fe $2p_{3/2}$ and $2p_{1/2}$ spectra appear at 711.0 and 723.5 eV, respectively, for ex-$CuFeO_2$ and ex-$CuFe_2O_4$. The peak positions indicate that oxidized Fe species are present on the surface of both catalysts, but that ex-$CuFeO_2$ is more reduced because of dominant peaks at 710.3 eV, indicating Fe^{2+}. On the other hand, a small, lower binding energy of 708 eV is only observed in ex-$CuFeO_2$, attributable to χ-Fe_5C_2 peak [35] formed during CO_2 hydrogenation. The XPS spectra of C 1p in Fig. S6c and d indicate that ex-$CuFeO_2$ contains carbonate species and carbon–carbon chains, while ex-$CuFe_2O_4$ contains only carbonate peaks. Hence, both XRD and XPS indicate the formation of the χ-Fe_5C_2 phase during the reaction only in ex-$CuFeO_2$ catalyst.

Our attempts to positively identify χ-Fe_5C_2 formation by XRD and XPS were only partly successful because XRD is not that sensitive for the materials of low crystallinity and XPS provides only near-surface information. Hence, X-ray absorption near-edge structure (XANES) spectroscopy was employed, which is an element specific, low concentration-sensitive, crystallinity-independent and local bulk structure-determining probe. Fig. 4a displays the Fe K-edge XANES spectra of delafossite $CuFeO_2$ catalysts. As-prepared $CuFeO_2$ has the same edge-rising portion as the reference Fe_2O_3 in terms of energy and shape, denoting a Fe^{3+} state. When reduced with hydrogen, the spectrum is shifted to a lower energy, which is identical to Fe foil. The catalyst after CO_2 hydrogenation at 300 °C for 16 h seems to have a similar edge position to Fe foil, but the edge-rising features are clearly different from each other. Spinel $CuFe_2O_4$ and hematite Fe_2O_3 catalysts were also analyzed as shown in Fig. 4b and c. In the case of $CuFe_2O_4$, the edge-rising position in the spectrum of as-prepared sample is close to Fe_2O_3 and $CuFeO_2$, but the edge feature above 7124 eV is different because $CuFeO_2$ and $CuFe_2O_4$ have their unique arrangements of neighboring atoms around a central iron as shown in the structural models in Fig. S9 of SI. The reduced sample exhibits near-edge feature at the lower energy region of 7110–7122 eV, but crossing edge-rising feature is observed at 7123 eV. Unlike $CuFeO_2$, Fe^{3+} in $CuFe_2O_4$ is reduced only to $Fe\delta^+$ rather than Fe^0. Moreover, the Fe state does not change after the reaction. The Fe_2O_3 catalyst shows close similarity to Fe foil when treated with hydrogen. The used Fe_2O_3 catalyst exhibits distinctly different XANES spectrum as compared to the reduced sample. For more detailed analysis, the derivative spectra of normalized absorbance are compared for all catalysts after the reaction in Fig. 4d. The Fe K-edge XANES spectrum of the used $CuFeO_2$ catalyst is very similar to that of the reference Hägg iron carbide (χ-Fe_5C_2) prepared by the reported method [36,37]. However, $CuFe_2O_4$ and Fe_2O_3 exhibit entirely different spectra from that of Hägg iron carbide. The study of Cu K-edge

XANES exhibits the full reduction of Cu^{+} in $CuFeO_2$ and Cu^{2+} in $CuFe_2O_4$ to Cu^0 state, which is maintained during the reaction (Fig. S10).

4. Discussion

Results of H_2-TPR, XRD, XPS and XANES analyses provide a consistent picture of the structural evolution of the catalysts from the precursor state to post-reaction as follows. Compared with Fe_2O_3 and $CuFe_2O_4$, Fe^{3+} in delafossite $CuFeO_2$ is reduced to Fe^0 to the greatest extent in the pre-reduction at 400 °C in H_2. This reduced state seems to play an essential role to form Hägg carbide *in situ* during the CO_2 hydrogenation reaction, which is the known active phase of iron-based catalysts in CO-FT synthesis and appears to be the active phase of CO_2 hydrogenation as well. The presence of copper in the catalyst is important to help Fe^{3+} readily reduced as is well established in CO-FT synthesis over iron-based catalysts [38]. However, we have demonstrated that the nature of precursor is critical in the reduction process. References of Cu_2O-Fe_2O_3 and spinel $CuFe_2O_4$ show only marginal promotional effects by copper although they also contain copper in separate phases or in a single phase, respectively. The origin of the different reducibility among the different precursors is not obvious. The spinel $CuFe_2O_4$ is usually synthesized at a high temperature over 800 °C and highly stable in static conditions with both metals in the fully oxidized states of Cu^{2+} and Fe^{3+}. But Cu in $CuFeO_2$ is in the intermediate oxidation state of Cu^{+}, and thus it may be thermodynamically less stable against reduction. Kinetically, it was reported that the rate constant at 543 K for the reduction to α-Fe was *ca.* 3.5 times higher for $CuFeO_2$ compared to $CuFe_2O_4$ [39]. Thus, swift reduction and *in-situ* carburization of $CuFeO_2$ during the reaction forms effectively the Hägg carbide, the known active catalytic phase for FT synthesis. In addition, 0.03% of Na was detected in the ICP analysis of the catalyst. Hence, a synergistic effect between the carbide phase and the small amount of alkali promotor seems responsible for the selective formation of heavier hydrocarbons. Relative to the Fe_2O_3-derived catalyst, the delafossite-derived catalyst shows improved higher hydrocarbon (C_5^{+}) selectivity from ~2% to ~65%, and increased olefin to paraffin ratio, whereas methane selectivity is greatly suppressed from ~60% to 2–3%.

5. Conclusions

Delafossite-$CuFeO_2$ becomes a precursor to Cu—Fe catalysts that produce higher liquid hydrocarbons with a selectivity of ~65%, an olefin-to-paraffin ratio of ~7.3, and minimal methane selectivity of 2–3%. This represents a typical product distribution obtained from FT synthesis from CO over efficient iron-based catalysts. This represents the first demonstration that liquid fuels and olefins of high value and large market could be obtained from CO_2, the most troublesome greenhouse gas. The unique role of delafossite-$CuFeO_2$ as the catalyst precursor is attributed to the swift reduction and selective carburization to form the Hägg iron carbide (χ-Fe_5C_2), which is the active catalytic phase for the formation of higher hydrocarbons in CO_2 hydrogenation. Other precursors like Cu_2O-Fe_2O_3 and $CuFe_2O_4$ are not effective in the formation of the active phase although they contain copper. We believe the new catalyst breaks through the limitation of CO_2-based FT synthesis and will open the avenue for new opportunity for recycling CO_2 into valuable fuels and chemicals.

Acknowledgement

This work was supported by Brain Korea Plus Program of Ministry of Education, Korean Center for Artificial Photosynthesis (NRF-2011-C1AAA0001-2011-0030278), the Basic Science Grant (NRF-2015R1A2A1A10054346), Climate Change Response project (2015M1A2A2074663) funded by MISIP and Project No. 10050509 funded by MOTIE of Republic of Korea.

Appendix A. Supplementary data

Supplementary data associated with this article can be found, in the online version, at http://dx.doi.org/10.1016/j.apcatb.2016.09.072.

References

[1] X.G. Lim, Nature 526 (2015) 628–630.
[2] D. Preti, C. Resta, S. Squarcialupi, G. Fachinetti, Angew. Chem. Int. Ed. 50 (2011) 12551–12554.
[3] N.A.M. Razali, K.T. Lee, S. Bhatia, A.R. Mohamed, Renew. Sustain. Energy Rev. 16 (2012) 4951–4964.
[4] M. He, Y. Sun, B. Han, Angew. Chem. Int. Ed. 52 (2013) 9620–9633.
[5] R.W. Dorner, D.R. Hardy, F.W. Williams, H.D. Willauer, Energy Environ. Sci. 3 (2010) 884–890.
[6] G. Centi, E.A. Quadrelli, S. Perathoner, Energy Environ. Sci. 6 (2013) 1711–1731.
[7] U. Rodemerck, M. Holena, E. Wagner, Q. Smejkal, A. Barkschat, M. Baerns, ChemCatChem 5 (2013) 1948–1955.
[8] S. Perathoner, G. Centi, ChemSusChem 7 (2014) 1274–1282.
[9] M.V. Landau, R. Vidruk, M. Herskowitz, ChemSusChem 7 (2014) 785–794.
[10] S. Saeidi, N.A.S. Amin, M.R. Rahimpour, J. CO_2 Util. 5 (2014) 66–81.
[11] F. MacDonald, Science Alert, 27 Apr. 2015, http://www.sciencealert.com/audi-have-successfully-made-diesel-fuel-from-air-and-water.
[12] J. Luo, J.-H. Im, M.T. Mayer, M. Schreier, M.K. Nazeeruddin, N.-G. Park, S.D. Tilley, H.J. Fan, M. Grätzel, Science 345 (2014) 1593–1596.
[13] K. Sivula, R. van de Krol, Nat. Rev. Mater. 1 (2016) 15010.
[14] Y.J. Jang, I. Jeong, J. Lee, J. Lee, M.J. Ko, J.S. Lee, ACS Nano 10 (2016) 6980–6987.
[15] T. Sakakura, J.-C. Choi, H. Yasuda, Chem. Rev. 107 (2007) 2365–2387.
[16] W. Wang, W. Wang, X. Ma, J. Gong, Chem. Soc. Rev. 40 (2011) 3703–3727.
[17] G. Kishan, M.-W. Lee, S.-S. Nam, M.-J. Choi, K.-W. Lee, Catal. Lett. 56 (1998) 215–219.
[18] H. Ando, Y. Matsumura, Y. Souma, J. Mol. Catal. A 154 (2000) 23–29.
[19] L.M. Chew, P. Kangvansura, H. Ruland, H.J. Schulte, C. Somsen, W. Xia, G. Eggeler, A. Worayingyong, M. Muhler, Appl. Catal. A 482 (2014) 163–170.
[20] F. Ding, A. Zhang, M. Liu, X. Guo, C. Song, RSC Adv. 4 (2014) 8930–8938.
[21] M. Al-Dossary, A.A. Ismail, J.L.G. Fierro, H. Bouzid, Appl. Catal. B 165 (2015) 651–660.
[22] S.R. Yan, K.-W. Jun, J.-S. Hong, M.-J. Choi, K.-W. Lee, Appl. Catal. A 194–195 (2000) 63–70.
[23] S. Li, H. Guo, C. Luo, H. Zhang, L. Xiong, X. Chen, L. Ma, Catal. Lett. 143 (2013) 345–355.
[24] X. Qiu, M. Liu, K. Sunada, M. Miyauchi, K. Hashimoto, Chem. Commun. 48 (2012) 7365–7367.
[25] M.M. Moharam, M.M. Rashad, E.M. Elsayed, R.M. Abou-Shahba, J. Mater. Sci. Mater. El. 25 (2014) 1798–1803.
[26] Y. Dong, C. Cao, Y.-S. Chui, J.A. Zapien, Chem. Commun. 50 (2014) 10151–10154.
[27] A.M. Sukeshini, H. Kobayashi, M. Tabuchi, H. Kageyama, Solid State Ionics 128 (2000) 33–41.
[28] L. Lu, J.-Z. Wang, X.-B. Zhu, X.-W. Gao, H.-K. Liu, J. Power Sources 196 (2011) 7025–7029.
[29] H.M.T. Galvis, C.B. Khare, M. Ruitenbeek, A.I. Dugulan, K.P. de Jong, Science 335 (2012) 835–838.
[30] J.C. Park, D.H. Chun, J.-I. Yang, H.-T. Lee, S. Hong, G.B. Rhim, S. Jang, H. Jung, RSC Adv. 5 (2015) 44211–44217.
[31] E. de Smit, F.M. de Groot, R. Blume, M. Hävecker, A. Knop-Gericke, B.M. Weckhuysen, Phys. Chem. Chem. Phys. 12 (2010) 667–680.
[32] V.R.R. Pendyala, G. Jacobs, M.K. Gnanamani, Y. Hu, A. MacLennan, B.H. Davis, Appl. Catal. A 495 (2015) 45–53.
[33] H.-Y. Lin, Y.-W. Chen, C. Li, Thermochim. Acta 400 (2003) 61–67.
[34] V. Subramanian, E.S. Gnanakumar, D.-W. Jeong, W.-B. Han, C.S. Gopinath, H.-S. Roh, Chem. Commun. 49 (2013) 11257–11259.
[35] K. Cheng, V.V. Ordomsky, M. Virginie, B. Legras, P.A. Chernavskii, V.O. Kazak, C. Cordier, S. Paul, Y. Wang, A.Y. Khodakov, Appl. Catal. A 488 (2014) 66–77.
[36] C. Yang, H. Zhao, Y. Hou, D. Ma, J. Am. Chem. Soc. 134 (2012) 15814–15821.
[37] H. Park, D.H. Youn, J.Y. Kim, W.Y. Kim, Y.H. Choi, Y.H. Lee, S.H. Choi, J.S. Lee, ChemCatChem 7 (2015) 3488–3494.
[38] J.W. Bae, S.-J. Park, S.-H. Kang, Y.-J. Lee, K.-W. Jun, Y.-W. Rhee, J. Ind. Eng. Chem. 15 (2009) 798–802.
[39] Z.H. Chonco, A. Ferreira, L. Lodya, M. Claeys, E. van Steen, J. Catal. 307 (2013) 283–294.